Chinese Journal of
POLYMER SCIENCE

RESEARCH ARTICLE

https://doi.org/10.1007/s10118-022-2709-1
Chinese J. Polym. Sci. **2022**, *40*, 651–657

Self-nucleation of Patterned Polymer Thin Films Defined by Soft Lithography

Ze-Qian Wang, Yi-Meng Wang, Xing-Yu Wang, Bing-Hua Wang, Jing-Bo Chen*, Chang-Yu Shen, and Bin Zhang*

School of Materials Science & Engineering, Zhengzhou University, Zhengzhou 450002, China

Electronic Supplementary Information

Abstract The nucleation of crystals is often a determining step in the phase transition of materials, but it remains a challenge to control the density and specific location of nuclei simultaneously. Here we fabricated the isolated single crystals of uniform size with controlled number density and spatial distribution by self-nucleation of patterned dendritic crystals. Imprint lithography creates the periodic void space on the surface of poly(ethylene oxide)-*b*-poly(2-vinyl pyridine) (PEO-*b*-P2VP) block copolymer thin films and provides spatial redistribution of polymers, leading to the preferential nucleation and subsequent oriented growth of dendrites in the periodic arrays of imprinted lines. The morphology and thermal stability of the patterned crystals can be adjusted by tuning embossing conditions (*e. g.*, temperature and pressure). Furthermore, in the self-nucleation technique, the annealing temperature and heating rate are used as the feedback parameters to map the number density and spatial distribution of regrown single crystals. Such PEO-*b*-P2VP crystalline pattern can be used as a versatile template for large-area manufacturing of selective metal patterns for electronic devices and other applications.

Keywords Self-nucleation; Imprint lithography; Atomic force microscopy; Crystallization pattern; Selective metal pattern

Citation: Wang, Z. Q.; Wang, Y. M.; Wang, X. Y.; Wang, B. H.; Chen, J. B.; Shen, C. Y.; Zhang, B. Self-nucleation of patterned polymer thin films defined by soft lithography. *Chinese J. Polym. Sci.* **2022**, *40*, 651–657.

INTRODUCTION

Nucleation is a determining step in crystallization.[1–6] Polymer crystallization is usually initiated by homogeneous or heterogeneous nucleation.[5–9] The former is nucleation by spontaneous arrangement of intramolecular or intermolecular chain segments, while the latter is nucleation on the nucleating agent surface or the phase interface.[10–13] In both cases, the nucleation site and crystal size are uncontrollable. Self-nucleation is an approach based on ordered structures survived after partial melting which act as nuclei to induce the regeneration of crystals.[14–20] Hu and Reiter *et al*.[21] reported a self-nucleation technique that enables the production of a multitude of regrown crystals with uniform size and orientation inherited from an initial single crystal. Recently, our group found that the competition between melting and lamellar thickening played a key role on the self-nucleation patterns in thin films.[22] However, compared to the rich and long-standing literature on the natural growth features (*e.g.*, spherulites, symmetric dendrites and single crystals), the growth of long-range oriented lamellar crystals still represents one of the key challenges in polymer nucleation.

Current strategies for controlling the oriented nucleation of polymer usually include flow,[23–32] epitaxial growth[33–35] and confined crystallization.[36–40] As a means of confined crystallization, imprinted lithography has emerged as a high-throughput and low-cost patterning tool capable of generating ordered micro- and nanofeatures in various polymeric materials.[41–43] The principle of imprinting is that a mold with micro- and nanostructures on its surface is pressed into a polymeric material above glass transition temperature or melting temperature, creating polymer-patterned surfaces.[42,44] For crystalline polymer, imprinting changes the geometrically confined space of polymer crystallization, for example, the film thickness and the width of the imprint lines, which has an impact on the shape, orientation, size and growth behavior of crystals.[45–47] So far, it remains a fascinating question to control specific location of nuclei in the predicted patterns.

In this study, the periodic arrays of dendrites were produced by means of the imprint lithography. The effects of the imprinting conditions (temperature and pressure) on the pattern uniformity and placement accuracy of lithographically defined oriented dendrites were presented. Further, we used self-nucleation technique as a tool to gain control over the number density and distribution of regrown single crystals. Combining with the imprinted dendritic crystals, this work

* Corresponding authors, E-mail: chenjb@zzu.edu.cn (J.B.C.)
E-mail: binzhang@zzu.edu.cn (B.Z.)

Special Issue: Ordered Structure of Polymers
Received December 30, 2021; Accepted February 4, 2022; Published online April 20, 2022

suggests the feasibility of tuning the long-range ordered pattern of polymer single crystals.

EXPERIMENTAL

Materials

PEO-*b*-P2VP diblock copolymer with PEO crystalline block (M_n=4000 g/mol, T_g=−67 °C) and P2VP amorphous block (M_n=2000 g/mol, T_g=87 °C) used in this work were supplied by Polymer Source Company in Canada. PEO-*b*-P2VP block copolymer was chosen as the research system because it can be used as a template to achieve various metal patterns.[48] The polydimethylsiloxane (PDMS) soft template consists of patterns with protrusions and trenches width of 10 μm, which was obtained from Suzhou Wenhao Microfluidic Technology Co., LTD. Toluene and $HAuCl_4$ were purchased from Sigma-Aldrich. The nominal melting temperature of a low molecular weight PEO (M_n=4000 g/mol) has been reported to be about 51 °C.[49]

PEO-*b*-P2VP Film Preparation and Patterning Process

PEO-*b*-P2VP was dissolved in toluene at 105 °C to make a solution of 0.5 wt% concentration. Then, the homogeneous solution was deposited onto a silicon substrate (P100 type, UV treated for 40 min before being placed on the spin-coater) and rotated for 120 s at a speed of 4000 r/min by a KW-4A spin-coater (Institute of Microelectronics, Chinese Academy of Sciences, China) to prepare thin films.

The experimental protocol is presented in Fig. S1 (in the electronic supplementary information, ESI). The films were first heated to imprinting temperature (T_p) and kept for 10 min. Subsequently, the samples were imprinted using PDMS template at T_p for 10 s under pressure of 0.02–0.20 MPa. Then the systems were quenched directly to room temperature before releasing the pressure and removing the mold (The imprint process is outlined in Fig. S2 in ESI). The films continued to crystallize isothermally at room temperature. Finally, they were heated from room temperature to T_s at a heating rate (V_h), held there for t_s and cooled at 10 °C/min down to 42 °C for t_{c2}. The resulting self-nucleation samples were examined by AFM after quenching to room temperature and a selective washing procedure. The washing process is as follows: the films were washed by dropping a hot toluene solvent of 18 °C onto the samples for 1 s and then dried in a flow of nitrogen.

Gold Deposition

The PEO-*b*-P2VP crystalline template-coated wafer was immersed in a $HAuCl_4$ aqueous solution of 1.0 wt% concentration for 24 h to allow the P2VP segment to couple with gold ions. Then the film was treated with oxygen plasma at a power of 80 W for 5 min to remove the polymer and reduce the gold ions. Finally, the gold particles were heated to 450 °C for 10 min to form a two-dimensional pattern.

Characterization

The morphology of the film was observed using an Olympus BX-53M optical microscope (Olympus, Tokyo, Japan) equipped with a Linkam LTS-420 hot stage (Linkam Scientific Instruments, Tadworth, UK). AFM topographic images were acquired with a Dimension Icon (Brucker Instruments) in peak-force mold. Conductivity measurement of gold particles was carried out by the same equipment in PF-TUNA mode.

RESULTS AND DISCUSSION

In order to control the orientation of polymer crystals, much of the previous work focused on crystallization behavior in a geometrically confined space produced by soft lithographic techniques.[50–53] It was found that film thickness, imprinting temperature (T_p), holding time, imprinting force and mold geometry all influence the nucleation and subsequent growth of crystalline polymer patterns.[46,47] Notably, the effect of soft lithographic on nucleation and growth of the single layer of flat-on lamellae has rarely been reported.

Fig. 1 displays the morphologies of PEO-*b*-P2VP thin films prepared under different embossing conditions using PDMS mold. The T_p dependence of crystal shape was firstly investigated. By heating the film close to the melting point of PEO (*e.g.*, T_p=50 °C), a continuous film accompanied by a few approximately circular holes with a diameter about of 2.5 μm was formed, due to the relatively long relaxation time of polymer chain at the nanoscale (see Fig. 1a). When T_p=60 °C, the polymer was pressed into the trenches of the PDMS mold owing to the enhanced motility of molecular chains, resulting in the preferential nucleation and subsequent growth of dendrites along the periodic arrays of imprinted lines (see Fig. 1b). It is interesting to observe that the growth direction of main branches is parallel to the imprinted lines. Upon increasing T_p to a higher temperature (90 °C), the chain mobility is enhanced significantly, which enables the polymer to flow and fill the trenches of mold. Because of a strongly reduced nucleation probability of polymers confined in the isolated monolayer, crystallization starts always in the thicker regions, *e.g.*, at the center of the line. Then branches grow towards the thinner regions (the gaps), forming an oriented crystal pattern, which was confirmed by optical micrographs in Fig. S3 (in ESI).

Next, the imprint pressure was also used to improve the spatial accuracy of the printed features. When increasing pressure from 0.05 MPa to 0.15 MPa (see Figs. 1d–1f), polymer materials were all pressed into the mold trenches, resulting in an array of oriented dendritic lamellae. At higher temperature or pressure, the remaining thin resist layer in the compressed area likely becomes too thin, thus the crystals usually grow with diffusion-limited morphologies (*e.g.*, seaweeds and dendrites).[54] In addition, we can find that the morphology of side-branches transition from the seaweed to dendritic is becoming apparent and only few side-branches are formed with the increase of temperature and pressure, because the density of side branches on the inverse of the residue layer thickness.[55] The above results indicate that these imprinted dendritic crystals exhibit dependence of temperature and film thickness.

To vary the orientation of dendrites, imprinting molds with other geometric structures such as sigmoid (see Figs. 1g and 1h) and circular template (see Fig. 1i) were applied, respectively. The dendrite axis was always along the direction of the mold trenches, which provides more possibilities for the subsequent regulation of nucleation locations and orientation of regrown crystals. By controlling the imprinting conditions, we have successfully prepared long-range oriented lamellar crystals with different shapes and orientations, paving the road for controlling locations of nuclei and regenerated crystals.

https://doi.org/10.1007/s10118-022-2709-1

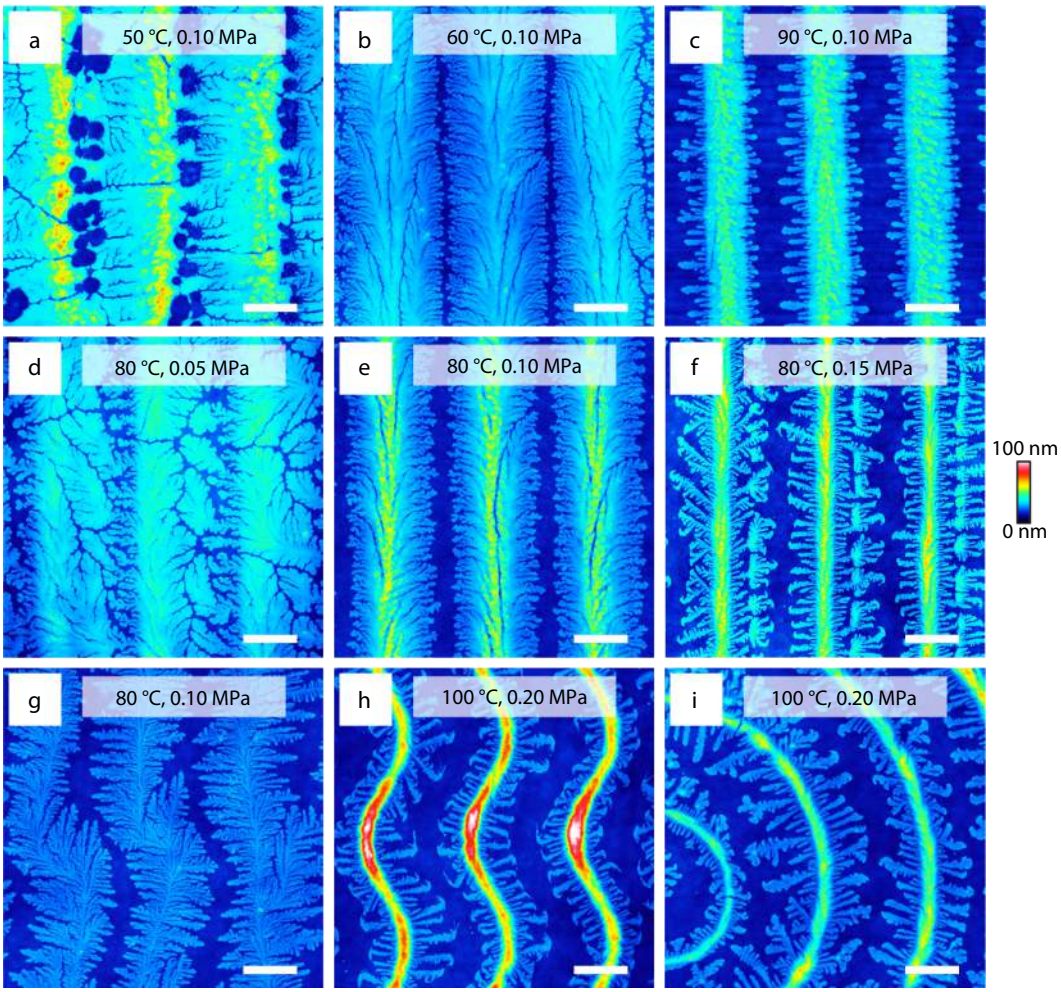

Fig. 1 Temperature and pressure dependence of imprinted crystallization morphology. AFM height images of the PEO-*b*-P2VP imprinted at different temperatures: (a) 50 °C, (b) 60 °C and (c) 90 °C with the pressure of 0.10 MPa. AFM height images of the PEO-*b*-P2VP imprinted using different pressures: (d) 0.05 MPa, (e) 0.10 MPa and (f) 0.15 MPa at 80 °C. AFM images showing the morphologies of PEO-*b*-P2VP patterns imprinted with different PDMS templates (g, h) sigmoid template, (i) circular template, respectively. The size of the scale bar is 10 μm.

Previous studies suggested that the number density and spatial distribution of crystals could be tuned by controlling the annealing temperature (T_s).[56] Fig. 2(a) shows the patterned tree-like dendritic crystals prepared after the thin film (~14 nm) being imprinted at 80 °C for 10 s and then cooling to room temperature. For T_s=44.5 °C (see Fig. 2b), an extremely high nucleation density was found on locations of initial main branches but few crystals could be found in the region of initial side branches. With rising T_s to 45 °C, the number density of regrown crystals decreased and some isolated crystals appeared in the region of initial main branches (see Fig. 2c).

Fig. 2(d) illustrates the height diagrams of crystallization patterns prepared at T_s=44.5 and 45 °C. We found that the crystals prepared at T_s=45 °C are twice the thickness of that at 44.5 °C, indicating that a secondary lamellar layer initiated on top of a basal lamella. The number density of such secondary lamellar crystals depends on the thickness of imprinted line, because the possibility of polymer chain diffusion on the fold surface increases with film thickness. The above results disclosed that the thermodynamically most stable parts of the initial dendrite were mainly located on the main branches. An evolution of the oriented arrays of recrystallization morphology from continuous to discontinuous linear pattern was realized by increasing seeding temperature. Furthermore, it appears that the specific localization of self-nuclei needs further study.

The competition between melting and recrystallization, which is responsible for the variations in the patterns of self-nucleation, is also related to the heating rate (V_h).[56] For V_h= 1 °C/min, as shown in Fig. 3(a), a higher number density of single crystals with uniform size and shape emerged. When increasing V_h to 2 and 5 °C/min, the number density of regrown crystals decreased significantly (see Figs. 3b and 3c). The size distributions of the single crystals induced at 1, 2 and 5 °C/min were analyzed, and then Gaussian fitting gave the average areas of 1.3±0.3, 2.0±0.5 and 3.4±0.8 μm^2, respectively, as summarized graphically in Fig. 3(d). For higher V_h, crystals tend to melt and fewer seeds remained during the heating process. Thus, sufficient molecular chains in the molten state were provided to the growth of crystals, leading to a larger crystal size. While a small particle size generated at a

https://doi.org/10.1007/s10118-022-2709-1

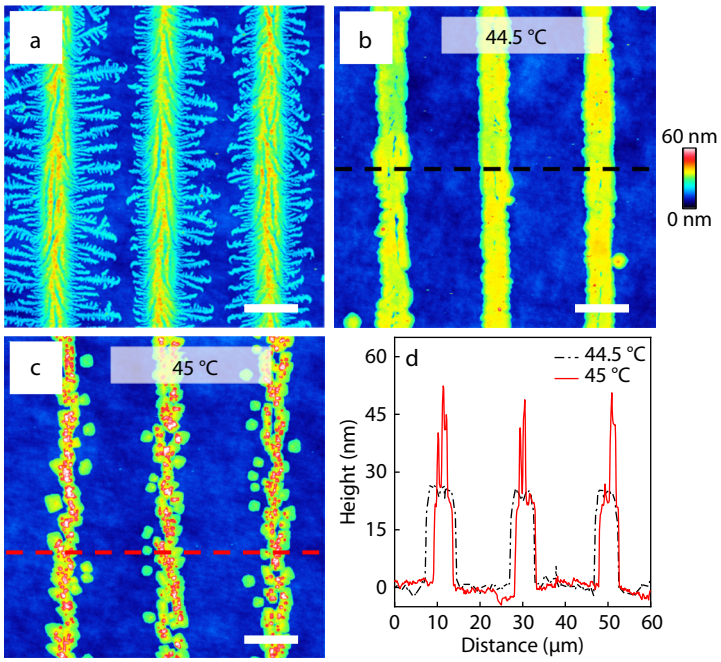

Fig. 2 The effect of seeding temperature on crystallization patterns of imprinted PEO-*b*-P2VP crystals. (a) AFM height image of the initial PEO-*b*-P2VP lamellae prepared after being imprinted at 80 °C and 0.10 MPa, followed by cooling to room temperature. (b, c) AFM images of the crystals obtained by annealing the initial lamellae at different temperatures (b) T_s=44.5 °C, (c) T_s=45 °C for 10 min with a heating rate of 30 °C/min, followed by isothermal recrystallization at 42 °C for 3 h. (d) Cross-section profiles along the directions of the dash lines in (b) and (c), respectively. The size of the scale bar is 10 μm.

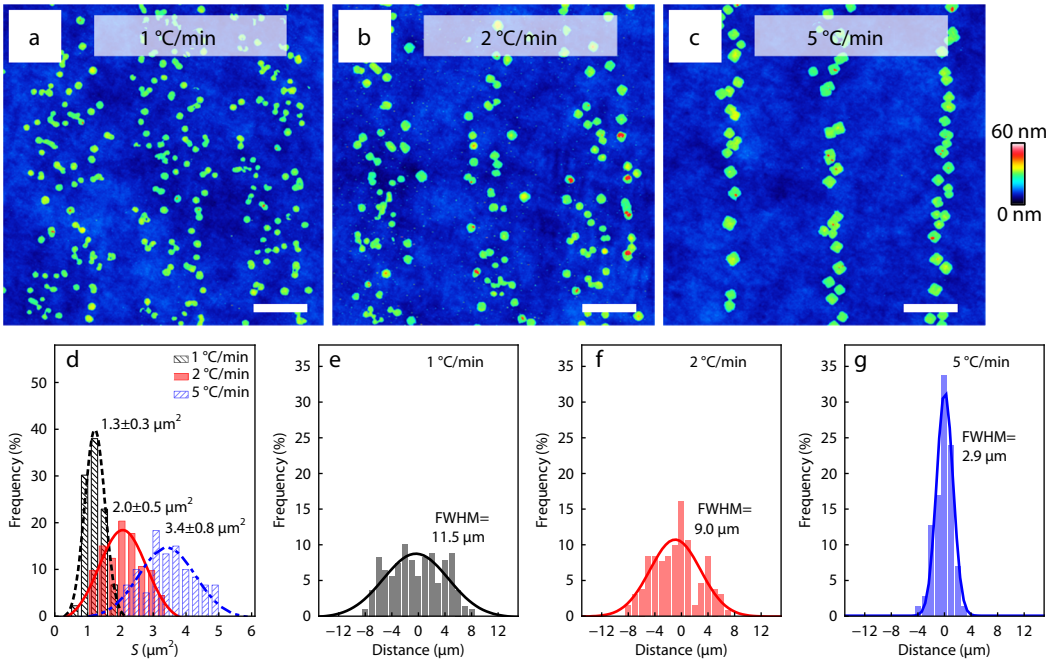

Fig. 3 The effect of heating rate on crystallization patterns of imprinted PEO-*b*-P2VP crystals. AFM height images of the PEO-*b*-P2VP crystals prepared after annealing initial lamellae (Figure 2a) at 47 °C for 3 min with different heating rates of (a) 1, (b) 2 and (c) 5 °C/min, followed by isothermal recrystallization at 42 °C for 4 min. The size of the scale bar is 10 μm. Diagrams of (d) the size distribution and (e, f, g) the spatial distribution of the nucleation probability shown in (a, b, c).

low V_h resulted from the lack of material available for a large number of crystals growth simultaneously.

The spatial distribution of the nucleation probability was obtained by counting the number of crystals at the different distances from center, and the probability distributions were fitted by Gaussian curve (see Figs. 3e–3g). Clearly, at higher V_h, the very high probability around the center of imprinted lines can be identified as a concentrated distribution due to

https://doi.org/10.1007/s10118-022-2709-1

only the most stable parts of main branches survived for further growing. Compared with the high V_h, an activation energy needed for thickening of crystals is smaller at low V_h,[22] thus less stable crystal (*e.g.*, side branches) favor thickening to become more perfect, which result in a more dispersed distribution of self-nuclei. Obviously, the periodic arrays of isolated PEO-*b*-P2VP crystals of uniform size with simultaneously controlled number density and spatial distribution of nucleation were prepared.

PEO-*b*-P2VP crystalline pattern can be used as a versatile template for manufacturing of metal patterns. Fig. 4(a) displays the crystallization patterns prepared by imprinting and self-nucleation. Then $[AuCl_4]^{2-}$ were crosslinked onto P2VP segments by immersing the crystals in $HAuCl_4$ solution, since the pyridine groups in P2VP segments can be coupled with $[AuCl_4]^{2-}$ *via* coordinate bonding. Subsequently, the surrounding polymer matrix was removed by the plasma, leaving Au particles on the Si substrate, as depicted in Fig. 4(b).

Compared with Fig. 4(a), no morphological difference can be found besides thickness. In other words, the gold pattern perfectly duplicates the crystal pattern which serve as a template, manifesting that the ideal metal patterns can be produced by tuning the crystallization conditions. In addition, the conductivity of an individual gold particle was measured by using conductive AFM in PF-TUNA mode. As illustrated in Figs. 4(c) and 4(d), the topography and conductive current images of Au particle are acquired simultaneously. AFM current map shows that Au particle exhibits extremely high conductivity, revealing the potential application of periodic arrays of isolated PEO-*b*-P2VP crystals in the synthesis of 2D metallic patterns.

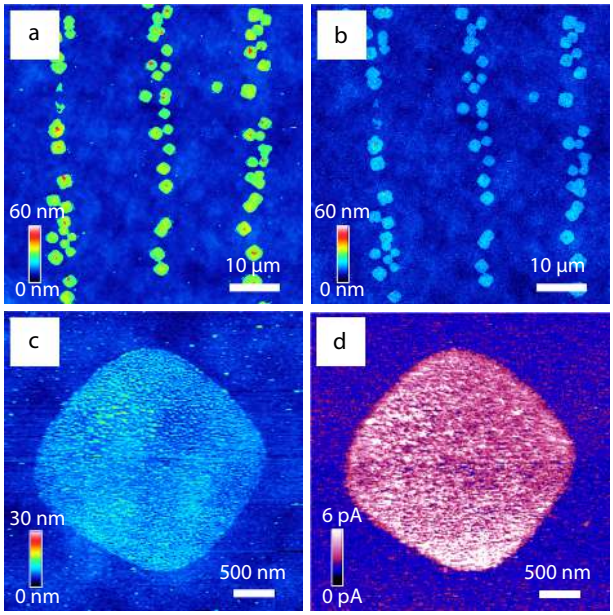

Fig. 4 AFM micrograph of metal pattern fabricated by imprint lithography and a self-nucleation process. (a) AFM height image of the PEO-*b*-P2VP crystals prepared after initial lamellae (in Fig. 2a) annealing at 47.5 °C with a heating rate of 5 °C/min for 3 min, followed by isothermal recrystallization at 42 °C for 3 min. (b, c) Surface topography of Au particle patterns prepared after metal complexation, plasma treatment and thermal annealing. (d) Contact current map of an individual gold particle in (c) collected at a voltage of 4 V.

CONCLUSIONS

In this work, the periodic arrays of PEO-*b*-P2VP isolated single crystals of uniform size with simultaneously controllable number density and spatial distribution of nuclei were prepared by self-nucleation of patterned dendritic crystals. In imprinting process, periodic arrangement of dendritic crystals appeared at higher imprinting temperature and pressure, and the morphology of side branches transformed from the seaweed to dendrite. Upon self-nucleation, the recrystallization morphology changing from continuous to discontinuous linear pattern was realized by increasing annealing temperature. The important parameters for the recrystallization pattern, such as the density and spatial distribution of nuclei, can be easily tuned by changing heating rate (1–5 ℃/min). This approach provides a strategy for the preparation of large-area multi-ordered crystallization patterns, which can be used for the manufacturing of metallic patterns for electronic devices and other applications.

NOTES

The authors declare no competing financial interest.

Electronic Supplementary Information

Electronic supplementary information (ESI) is available free of charge in the online version of this article at http://doi.org/10.1007/s10118-022-2709-1.

ACKNOWLEDGMENTS

This work was financially supported by the National Natural Science Foundation of China (Nos. 51973202, 51773182, U1804144, 52003247 and 11872338), the China Postdoctoral Science Foundation (No. 2020M682340), the Young Outstanding Teachers of University in Henan Province (No. 2019GGJS003), the Postdoctoral Research Grant in Henan Province (No. 201901009), and the Startup Research Fund of Zhengzhou University (No. 32211191).

REFERENCES

1 Binsbergen, F. L. Orientation-induced nucleation in polymer crystallization. *Nature* **1966**, *211*, 516–517.
2 Mercier, J. P. Nucleation in polymer crystallization: a physical or a chemical mechanism. *Polym. Eng. Sci.* **1990**, *30*, 270–278.
3 Xu, J.; Reiter, G.; Alamo, R. G. Concepts of nucleation in polymer crystallization. *Crystals* **2021**, *11*, 304.
4 Hu, W. The physics of polymer chain-folding. *Phys. Rep.* **2018**, *747*, 1–50.
5 Wang, B.; He, K.; Lu, Y.; Zhou, Y.; Chen, J.; Shen, C.; Chen, J.; Men, Y.; Zhang, B. Nucleation mechanism for form II to I polymorphic transformation in polybutene-1. *Macromolecules* **2020**, *53*, 6476–6485.
6 Qiao, Y.; Wang, Q.; Men, Y. Kinetics of nucleation and growth of

form II to I polymorphic transition in polybutene-1 as revealed by stepwise annealing. *Macromolecules* **2016**, *49*, 5126–5136.
7 Schick, C.; Androsch, R.; Schmelzer, J. W. P. Homogeneous crystal nucleation in polymers. *J. Phys.: Condens. Matter* **2017**, *29*, 453002.
8 Lu, Y.; Lyu, D.; Cavallo, D.; Men, Y. Enhanced beta to alpha recrystallization in beta isotactic polypropylene with different thermal histories. *Polym. Cryst.* **2019**, *2*, e10040.
9 Hou, C.; Wan, R.; Sun, X.; Ren, Z.; Li, H.; Yan, S. The development of an abnormal isotactic polypropylene spherulite: morphology and kinetics. *Polym. Cryst.* **2020**, *3*, e10157.
10 Binsbergen, F. L. Natural and artificial heterogeneous nucleation in polymer crystallization. *J. Polym. Sci., Polym. Symp.* **1977**, *59*, 11–29.
11 Li, L.; Xin, R.; Li, H.; Sun, X.; Ren, Z.; Huang, Q.; Yan, S. Tacticity-dependent epitaxial crystallization of poly(L-lactic acid) on an oriented polyethylene substrate. *Macromolecules* **2020**, *53*, 8487–8493.
12 Li, L.; Hu, J.; Li, Y.; Huang, Q.; Sun, X.; Yan, S. Evidence for the soft and hard epitaxies of poly(L-lactic acid) on an oriented polyethylene substrate and their dependence on the crystallization temperature. *Macromolecules* **2020**, *53*, 1745–1751.
13 Liu, Z.; Zheng, G.; Shi, H.; Liu, C.; Mi, L.; Li, Q.; Liu, X. Simultaneous enhancement of toughness and strength of stretched *i*PP film *via* tiny amount of β-nucleating agent under "shear-free" melt-extrusion. *Chinese J. Polym. Sci.* **2021**, *39*, 1481–1488.
14 Blundell, D. J.; Keller, A.; Kovacs, A. J. A new self-nucleation phenomenon and its application to the growing of polymer crystals from solution. *J. Polym. Sci., Part B: Polym. Lett.* **1966**, *4*, 481–486.
15 Reiter, G. Some unique features of polymer crystallisation. *Chem. Soc. Rev.* **2014**, *43*, 2055–2065.
16 Zhou, T; Yang, H.; Ning, N.; Xiang, Y; Du, R; Fu, Q. Partial melting and recrystallization of isotactic polypropylene. *Chinese J. Polym. Sci.* **2010**, *28*, 77–83.
17 Sangroniz, L.; Cavallo, D.; Müller, A. J. Self-Nucleation effects on polymer crystallization. *Macromolecules* **2020**, *53*, 4581–4604.
18 Chen, E.; Weng, X.; Zhang, A.; Mann, I.; Harris, F. W.; Cheng, S. Z. D.; Stein, R.; Hsiao, B. S.; Yeh, F. Primary nucleation in polymer crystallization. *Macromol. Rapid Commun.* **2001**, *22*, 611–615.
19 Fillon, B.; Thierry, A.; Wittmann, J. C.; Lotz, B. Self-nucleation and recrystallization of polymers. Isotactic polypropylene, β phase: β-α conversion and β-α growth transitions. *J. Polym. Sci., Part B: Polym. Phys.* **1993**, *31*, 1407–1424.
20 Jiang, J.; Zhuravlev, E.; Hu, W.; Schick, C.; Zhou, D. The effect of self-nucleation on isothermal crystallization kinetics of poly(butylene succinate) (PBS) investigated by differential fast scanning calorimetry. *Chinese J. Polym. Sci.* **2017**, *35*, 1009–1019.
21 Xu, J.; Ma, Y.; Hu, W.; Rehahn, M.; Reiter, G. Cloning polymer single crystals through self-seeding. *Nat. Mater.* **2009**, *8*, 348–353.
22 Wang, B.; Tang, S.; Wang, Y.; Shen, C.; Reiter, R.; Reiter, G.; Chen, J.; Zhang, B. Systematic control of self-seeding crystallization patterns of poly(ethylene oxide) in thin films. *Macromolecules* **2018**, *51*, 1626–1635.
23 Cui, K.; Ma, Z.; Tian, N.; Su, F.; Liu, D.; Li, L. Multiscale and multistep ordering of flow-induced nucleation of polymers. *Chem. Rev.* **2018**, *118*, 1840–1886.
24 Zhang, B.; Chen, J.; Ji, F.; Zhang, X.; Zheng, G.; Shen, C. Effects of melt structure on shear-induced β-cylindrites of isotactic poly propylene. *Polymer* **2012**, *53*, 1791–1800.
25 Zhang, B.; Chen, J.; Zhang, X.; Shen, C. Formation of β-cylindrites under supercooled extrusion of isotactic polypropylene at low shear stress. *Polymer* **2011**, *52*, 2075–2084.
26 Zhang, B.; Chen, J.; Cui, J.; Zhang, H.; Ji, F.; Zheng, G.; Heck, B.; Reiter, G.; Shen, C. Effect of shear stress on crystallization of isotactic polypropylene from a structured melt. *Macromolecules* **2012**, *45*, 8933–8937.
27 Chen, J.; Wang, B.; Sun, T.; Xu, J.; Chen, J.; Zhang, B. Transformation from form II to form I accelerated by oriented lamellae in polybutene-1. *Polymer* **2019**, *185*, 121966.
28 Lu, Y.; Li, H.; Wei, H.; Wang, B.; Shen, C.; Zhang, B.; Chen, J. Influence of melt structure on form II to I phase transition of polybutene-1 under shear flow. *Polymer* **2020**, *199*, 122562.
29 Zhang, B.; Chen, J.; Freyberg, P.; Reiter, R.; Mülhaupt, R.; Xu, J.; Reiter, G. High-temperature stability of dewetting-induced thin polyethylene filaments. *Macromolecules* **2015**, *48*, 1518–1523.
30 Zhang, H.; Wang, B.; Wang, G.; Shen, C.; Chen, J.; Reiter, G.; Zhang, B. Dewetting-induced alignment and ordering of cylindrical mesophases in thin block copolymer films. *Macromolecules* **2020**, *53*, 9631–9640.
31 Nie, Y.; Zhao, Y.; Matsuba, G.; Hu, W. Shish-kebab crystallites initiated by shear fracture in bulk polymers. *Macromolecules* **2018**, *51*, 480–487.
32 Nie, C.; Peng, F.; Xu, T.; Sheng, J.; Chen, W.; Li, L. A unified thermodynamic model of flow-induced crystallization of polymer. *Chinese J. Polym. Sci.* **2021**, *39*, 1489–1495.
33 Li, H.; Yan, S. Surface-induced polymer crystallization and the resultant structures and morphologies. *Macromolecules* **2011**, *44*, 417–428.
34 Cheng, S.; Hu, W.; Ma, Y.; Yan, S. Epitaxial polymer crystal growth influenced by partial melting of the fiber in the single-polymer composites. *Polymer* **2007**, *48*, 4264–4270.
35 Hu, W.; Frenkel, D.; Mathot, V. Simulation of shish-kebab crystallite induced by a single prealigned macromolecule. *Macromolecules* **2002**, *35*, 7172–7174.
36 Palacios, J. K.; Zhang, H.; Zhang, B.; Hadjichristidis, N.; Müller, A. J. Direct identification of three crystalline phases in PEO-*b*-PCL-*b*-PLLA triblock terpolymer by *In situ* hot-stage atomic force microscopy. *Polymer* **2020**, *205*, 122863.
37 Wang, H.; Keum, J. K.; Hiltner, A.; Baer, E. Confined crystallization of PEO in nanolayered films impacting structure and oxygen permeability. *Macromolecules* **2009**, *42*, 7055–7066.
38 Wang, H.; Keum, J. K.; Hiltner, A.; Baer, E.; Freeman, B.; Rozanski, A.; Galeski, A. Confined crystallization of polyethylene oxide in nanolayer assemblies. *Science* **2009**, *323*, 757–760.
39 Ma, M.; Guo, Y. Physical properties of polymers under soft and hard nanoconfinement: a review. *Chinese J. Polym. Sci.* **2020**, *38*, 565–578.
40 Huang, H.; Yi, G.; Zu, X.; Zhong, B.; Luo, H. Patterning of triblock copolymer film and its application for surface-enhanced Raman scattering. *Chinese J. Polym. Sci.* **2017**, *35*, 623–630.
41 Chou, S. Y.; Krauss, P. R.; Renstrom, P. J. Imprint lithography with 25-nanometer resolution. *Science* **1996**, *272*, 85–87.
42 Chou, S. Y.; Krauss, P. R.; Zhang, W.; Guo, L.; Zhuang, L. Sub-10 nm imprint lithography and applications. *J. Vac. Sci. Technol., B: Microelectron. Nanometer Struct.-Process., Meas., Phenom.* **1997**, *15*, 2897–2904.
43 Guo, L. J. Nanoimprint lithography: methods and material requirements. *Adv. Mater.* **2007**, *19*, 495–513.
44 Chou, S. Y.; Krauss, P. R.; Renstrom, P. J. Imprint of sub-25 nm vias and trenches in polymers. *Appl. Phys. Lett.* **1995**, *67*, 3114–3116.
45 Peng, L.; Deng, Y.; Yi, P.; Lai, X. Micro hot embossing of thermoplastic polymers: a review. *J. Micromech. Microeng.* **2013**, *24*, 013001.
46 Okerberg, B. C.; Soles, C. L.; Douglas, J. F.; Ro, H. W.; Karim, A.; Hines, D. R. Crystallization of poly(ethylene oxide) patterned by nanoimprint lithography. *Macromolecules* **2007**, *40*, 2968–2970.
47 Hu, Z.; Baralia, G.; Bayot, V.; Gohy, J. F.; Jonas, A. M. Nanoscale

https://doi.org/10.1007/s10118-022-2709-1

control of polymer crystallization by nanoimprint lithography. *Nano Lett.* **2005**, *5*, 1738–1743.
48 Yang, H.; Xu, L.; Li, X.; Zhang, X. One simple route to fabricate gold nanowire network films by using P2VP-*b*-PEO diblock copolymers as templates. *Mater. Chem. Phys.* **2009**, *114*, 525–529.
49 Cheng, S. Z. D.; Zhang, A.; Chen, J.; Heberer, D. P. Nonintegral and integral folding crystal growth in low-molecular mass poly(ethylene oxide) fractions. I. Isothermal lamellar thickening and thinning. *J. Polym. Sci., Part B: Polym. Phys.* **1991**, *29*, 287–297.
50 Kang, J. H.; Kim, K. S.; Kim, K. W. Molecular dynamics study on the effects of stamp shape, adhesive energy, and temperature on the nanoimprint lithography process. *Appl. Surf. Sci.* **2010**, *257*, 1562–1572.
51 Yang, Y.; Mielczarek, K.; Zakhidov, A.; Hu, W. Large molecular weight polymer solar cells with strong chain alignment created by nanoimprint lithography. *ACS Appl. Mater. Interfaces* **2016**, *8*, 7300–7307.
52 Aryal, M.; Trivedi, K.; Hu, W. Nano-confinement induced chain alignment in ordered P3HT nanostructures defined by nanoimprint lithography. *ACS Nano* **2009**, *3*, 3085–3090.
53 Yang, Y.; Mielczarek, K.; Aryal, M.; Zakhidov, A.; Hu, W. Nanoimprinted polymer solar cell. *ACS Nano* **2012**, *6*, 2877–2892.
54 Reiter, G.; Botiz, I.; Graveleau, L.; Grozev, N.; Albrecht, K.; Mourran, A.; Möller, M. Morphologies of polymer crystals in thin films. In *Progress in understanding of polymer crystallization*, Springer, Berlin Heidelberg New York, **2007**, p. 179–200.
55 Taguchi, K.; Miyaji, H.; Izumi, K.; Hoshino, A.; Miyamoto, Y.; Kokawa, R. Crystal growth of isotactic plystyrene in ultrathin films: film thickness dependence. *J. Macromol. Sci., Part B* **2002**, *41*, 1033–1042.
56 Wang, B.; Wang, G.; He, S.; Sun, T.; Chen, J.; Shen, C.; Zhang, B. Self-nucleation of β-form isotactic polypropylene lamellar crystals in thin films. *Macromolecules* **2021**, *54*, 11404–11411.

https://doi.org/10.1007/s10118-022-2709-1